Composite Structures 160 (2017) 560–573

Contents lists available at ScienceDirect

Composite Structures

journal homepage: www.elsevier.com/locate/compstruct

Adhesively-bonded GFRP-glass sandwich components for structurally efficient glazing applications

Carlos Pascual *, Jacopo Montali, Mauro Overend

Glass and Facade Technology Research Group, Department of Engineering, University of Cambridge, Trumpington Street, Cambridge CB2 1PZ, United Kingdom

ARTICLE INFO

Article history:
Received 5 August 2016
Revised 30 September 2016
Accepted 18 October 2016
Available online 18 October 2016

Keywords:
Adhesively-bonded connection
Analytical models
Glass
Glass fibre-reinforced polymer
Composite sandwich structure

ABSTRACT

Composite sandwich structures made of thick glass face sheets adhesively-bonded to glass fibre-reinforced polymer (GFRP) core profiles have the potential to outperform existing non-composite glazing configurations but their feasibility has yet to be investigated and there are no analytical models that describe their structural response. This paper presents the new analytical models for predicting deflections and strains in adhesively-bonded GFRP-glass sandwich beams. The new analytical models successfully account for: the shear deformations of the core and adhesive layers; the local bending of the constituent parts about their centroidal axes; and the global bending of the sandwich component as a whole. The deflections and strains predicted by analytical models are validated by finite element simulations and compared with the results of destructive tests performed on adhesively-bonded GFRP-glass beams in a four-point bending configuration. The analytical models were also evaluated for alternative GFRP-glass configurations tested by others. The GFRP-glass beams specially assembled in this study confirm the physical feasibility of constructing these proposed components.

1. Introduction

1.1. Motivation

Sandwich structures are layered components generally made of two thin, dense and stiff face sheets (traditionally metal or fibre-reinforced polymer laminates) separated by, and structurally bonded to, a thick, low density and less stiff core layer (traditionally metallic honeycomb, foam or balsa core). This arrangement results in a lightweight structure with much greater flexural rigidity than the sum of the individual constituent layers. Sandwich structures are therefore adapted for resisting bending loads, e.g. wind loads acting on building envelopes. In fact, sandwich components in building envelopes date back to the 1950s, when prefabricated lightweight and opaque sandwich panels, e.g. made of steel or aluminium face sheets adhesively-bonded to resin-reinforced paper honeycomb, were widespread in the American building construction market [1]. Over the last decades, the design intent of maximizing the transparency of building envelopes has increased the interest of architects for polymer-based sandwich components exhibiting different degrees of light transmittance. For short-span building applications, low-cost prefabricated sandwich components can be designed with transparent and high-durable unreinforced polymers, e.g. acrylic honeycomb cores bonded to outer acrylic face sheets [2]. However, the fabrication of large-span translucent sandwich components commonly requires laborious and costly hand lay-up processes, e.g. hand-laminated sandwich components made of an orthogonal grid of glass fibre-reinforced polymer (GFRP) core-webs and outer GFRP face sheets [3] [4]. Furthermore, in such GFRP sandwich components it is often necessary to fill the grid with opaque foam blocks (to prevent buckling of webs and face sheets) and to paint external surfaces (to improve the long-term durability) – thereby reducing or eliminating the light transmittance of the structures [3,4].

It is possible to devise load-bearing sandwich structures for building envelopes which simultaneously provide a high degree of transparency, structural efficiency, durability and thermal performance. In their most basic form these would consist of two monolithic and thick glass face sheets structurally bonded to GFRP pultruded core profiles (Fig. 1). In this configuration, light transmittance is largely unimpeded, the GFRP material is effectively protected from weathering and the air cavity between the two face sheets offers potential for high thermal insulation. This GFRP-glass sandwich concept involves a radical shift from the current use of glass in buildings envelopes – from its traditional use as inefficient infill panel to a robust and structurally efficient load-bearing component.

* Corresponding author.
E-mail address: cp570@cam.ac.uk (C. Pascual).

http://dx.doi.org/10.1016/j.compstruct.2016.10.059
0263-8223/

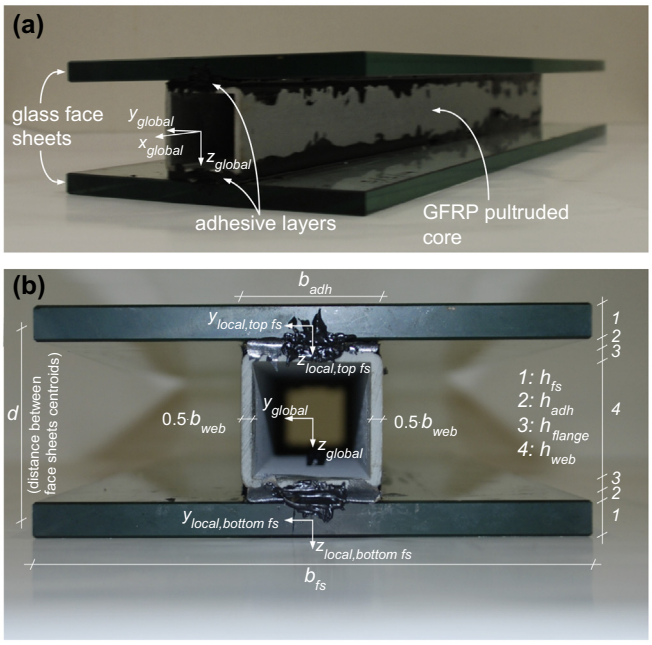

Fig. 1. (a) General view and (b) cross-section of the proposed adhesively-bonded GFRP-glass sandwich beam referred in the following as GFRP-DP490-glass beam.

1.2. Literature review

The idea of bonding fibre-reinforced polymers to glass components is not in itself new. Palumbo et al. [5] and Louter et al. [6,7] performed experimental research on glass beams reinforced in the tensile zone with adhesively-bonded fibre-reinforced polymers. Wurm [8] performed a basic experimental study of sandwich structures for facade applications made of pultruded GFRP core profiles adhesively-bonded to thin glass face sheets. Peters [9] and Knippers [4] investigated experimentally the feasibility of fabricating adhesively-bonded GFRP-glass façade panels and built mock-up specimens using structural adhesives DC993 (silicone) and 3M DP490 (epoxy). Polymeric foils made of TSSA (structural silicone) and SentryGlas® (ionomer) might be also candidate adhesives for bonding GFRP and glass components however autoclave lamination processes are required to produce the connection [10]. Tomasi et al. [11] concluded from the numerical modelling of GFRP-glass facades that adhesives with elastic modulus $E > 0.2$ GPa are required to achieve high degrees of composite action between GFRP and glass constituents. However adhesives that are sufficiently stiff to mobilise significant composite action, yet flexible enough to reduce stress concentrations and therefore minimize the risk of premature glass or adhesive failure, could provide an optimal solution for the design of safe and efficient adhesively-bonded glass-GFRP sandwich structures. Overend et al. [12] showed that the load-bearing capacities of adhesive connections can exceed those of equivalently sized bolted connections. This is largely due to the fact that adhesive connections generate smaller stress concentrations than those in similarly sized bolted connections and in addition adhesive bonding does not involve processes that weaken the glass such as the flaw-inducing process of drilling or the difficulties associated with thermally toughening of glass in the vicinity of a bolt hole [13] [14].

The deflections of adhesively-bonded sandwich components subjected to transverse loads (e.g. wind loads) result from the contribution of two coupled responses described analytically by Allen [15]: a local response in which the cross-sections of core and face sheets bend independently of each other about their own centroidal axes and a global response in which sandwich cross-section bends as a whole about its centroidal axis. The former response produces bending moments and shear forces in the core and face sheets cross-sections, whose sum is termed local bending moment, M_{local}, and local shear force, Q_{local}, respectively; and the latter response produces a bending moment and shear force on the whole sandwich cross-section, referred to as global bending moment, M_{global}, and global shear force, Q_{global}, respectively. However Allen's work considers the adhesive layers to be thin and with a high shear stiffness and therefore assumes these layers to have negligible shear deformations (henceforth referred to as shear-rigid). Another model developed by Natterer and Hoeft [16] captures the deflections of sandwich structures with relevant shear deformations in the adhesive layers (henceforth referred to as shear-flexible) but disregards the shear deformations of the core. Recently Osei-Antwi et al. [17] developed an analytical model for predicting the deflections of sandwich beams with multilayer shear-flexible cores, however the model is based on classical sandwich theory and therefore assumes thin face sheets and disregards local bending moments [18]. Similarly Overend et al. [19] developed an analytical model for predicting deflections of three-glass-ply laminated units with shear flexible adhesive interlayers however external glass laminates were assumed to be thin and local bending moments were disregarded. In recent experimental investigations Correia et al. [20] uses classical Euler-Bernoulli beam theory to investigate the deflections of adhesively-bonded sandwich beams with glass cores and GFRP face sheets – however predictions largely mismatched the experimental results for beams bonded with shear-flexible adhesives. There is currently no analytical means of calculating the load-deflection response of a sandwich component that considers both the shear flexibility of adhesive layers and cores and the local flexural rigidities of cores and face sheets. However such a model would constitute a valuable tool for the preliminary design of adhesively-bonded GFRP-glass sandwich envelopes such as envelopes based on the component proposed in this study – and in combination with other analytical models (e.g. thermal heat transfer), the influence of sandwich materials and geometry on the structural and thermal performance of building envelopes could be easily assessed.

1.3. Objectives

The objectives of this research are to extend Allen's work to adhesively-bonded sandwich structures with shear-flexible adhesive layers and cores and to demonstrate the feasibility and structural efficiency of the proposed sandwich component for building envelopes made of two thick glass face sheets structurally bonded to thin-wall pultruded GFRP core profiles. This paper, firstly, presents the new analytical models of the cross-sectional flexural rigidities and shear stiffness specifically developed for predicting the deflections and strains of sandwich structures subjected to transverse loads. Secondly, the elastic and shear moduli of the polymeric materials required for fabricating the proposed sandwich component are characterized from single-lap shear experiments (for the adhesive) and burn-off experiments (for the pultruded GFRP profiles). Thirdly, the validity of the new analytical models is evaluated by comparison with the results obtained from numerical modelling and from experimental destructive tests of three nominally identical adhesively-bonded GFRP-glass sandwich beams (Fig. 1) subjected to four-point bending. The analytical models developed in this paper are also tested by comparison with the experimental results obtained independently by Correia et al. [20] for an alternative adhesively-bonded GFRP-glass sandwich configuration.

2. New analytical models

2.1. Overview, sign convention and model assumptions

The new analytical models are intended as an aid in the structural design of the proposed sandwich components made of pultruded GFRP cores bonded to glass face sheets (Fig. 1) and can also be used for other sandwich configurations, e.g. glass beams strengthened with adhesively-bonded GFRP profiles as investigated by Correia et al. (Fig. 2) [20]. These new models extend Allen's work [15] to sandwich components with shear-flexible adhesive layers and for the purposes of this paper have been developed for structures subjected to four-point bending loads. First the kinematics of the local and global responses are described. Then the cross-sectional flexural rigidities and shear stiffness models are presented and the analytical solutions of the sandwich deflections and strains are obtained – see Appendix A for detailed development of the models and Appendix B for the notation used in this paper.

The sign convention adopted for the deflections (and its derivatives) follow the reference systems shown in Fig. 1 and the sign convention for the bending moments and shear forces is shown in Fig. 3. The following seven assumptions have been adopted in developing the new analytical models: 1) sandwich cross-section is double symmetric and is subjected to shear forces and bending moments alone, 2) in the local response face sheets and core bend with the same curvature, 3) sandwich materials are linear elastic, 4) flexural rigidities of adhesive layers about their own centroidal axes are disregarded, 5) adhesive and core-webs are shear-flexible and face sheets and core-flanges are shear-rigid, 6) contributions of core-webs to flexural rigidity and of core-flanges to shear stiffness – i.e. axial stresses (in core-webs) and shear stresses (in core-flanges) – are disregarded and 7) for ease of developing analytical models and analytical solutions of deflections and strains, shear strains in core-webs produced by Q_{local} are initially disregarded – in a subsequent stage these strains are estimated and an approximate solution of shear strains in core-webs is proposed.

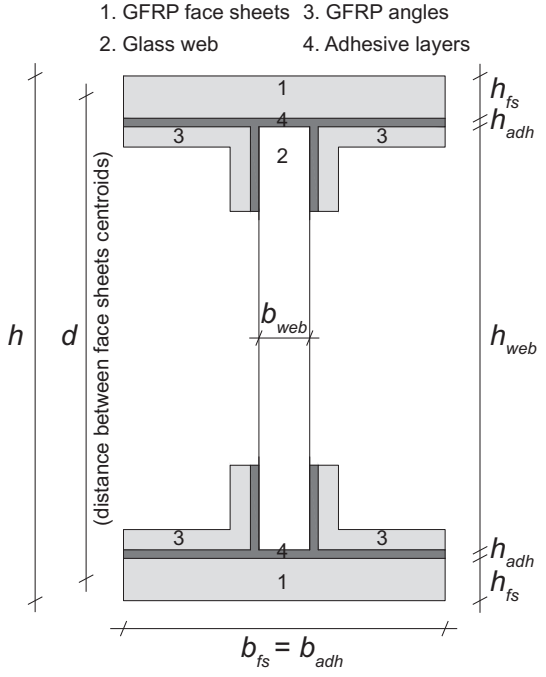

Fig. 2. Schematic cross-section of the two adhesively-bonded GFRP-glass sandwich beams investigated by Correia et al. [20] referred in the following as GFRP-Sikadur330-glass and GFRP-Sikaflex265-glass beams (not to scale).

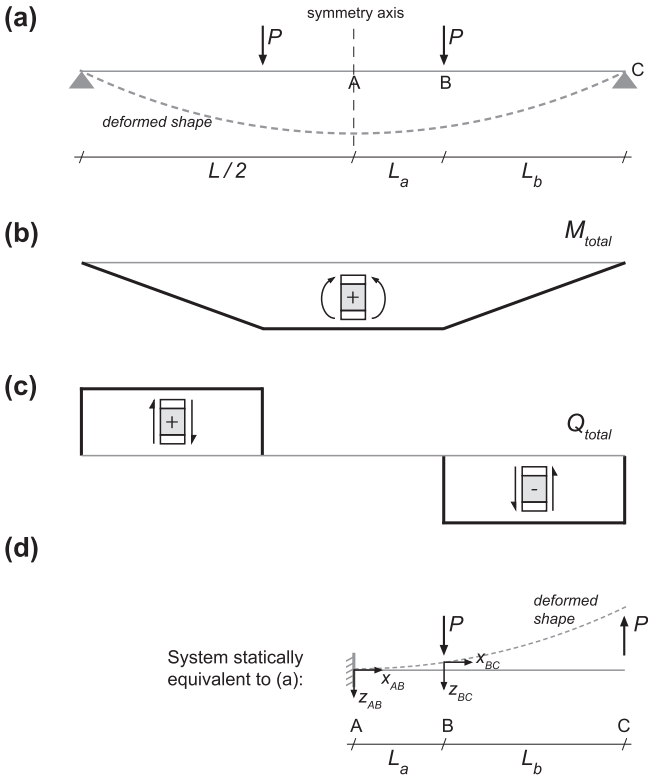

Fig. 3. (a) Four-point bending loading configuration, (b) total bending moments, (c) total shear forces and (d) equivalent static system. Note: symbols + and − indicate positive and negative sign convention.

2.2. Kinematics of sandwich cross-section

The total bending moments, M_{total}, and shear forces, Q_{total}, shown in Fig. 3 produce two cross-sectional responses described by the kinematics shown in Fig. 4: 1) A local response (Fig. 4b) in which cross-sections of the constituent layers bend about their respective centroidal axes and resist bending moments and shear forces – at a given sandwich cross-section, the sums of these bending moments and shear forces are referred as M_{local} and Q_{local}, respectively. This local response distorts the adhesive layers which transfer therefore shear stresses between face sheets and core – the integral of these stresses over the sandwich cross-sectional area equates to the global shear force Q_{global}. 2) A global response (Fig. 4c) in which sandwich cross-section bends as a whole about its centroidal axis and resists global bending moments M_{global} in equilibrium with Q_{global}. The total bending moments and the total shear forces are respectively given by the sum of the local and global bending moments and shear forces (see Eqs. (A.1) and (A.2)). Similarly, the total deflections result from the sum of the deflections due to the local and global responses, respectively termed w_{local} and w_{global}. The static systems, shear forces and bending moments, and axial and shear stresses produced by the local and global responses are shown in Fig. 5.

2.3. New models of flexural rigidities and shear stiffness

The new models of flexural rigidities and shear stiffness are developed in the Appendix A and the main results are reported here. The local flexural rigidity, D_{local}, and global flexural rigidity,

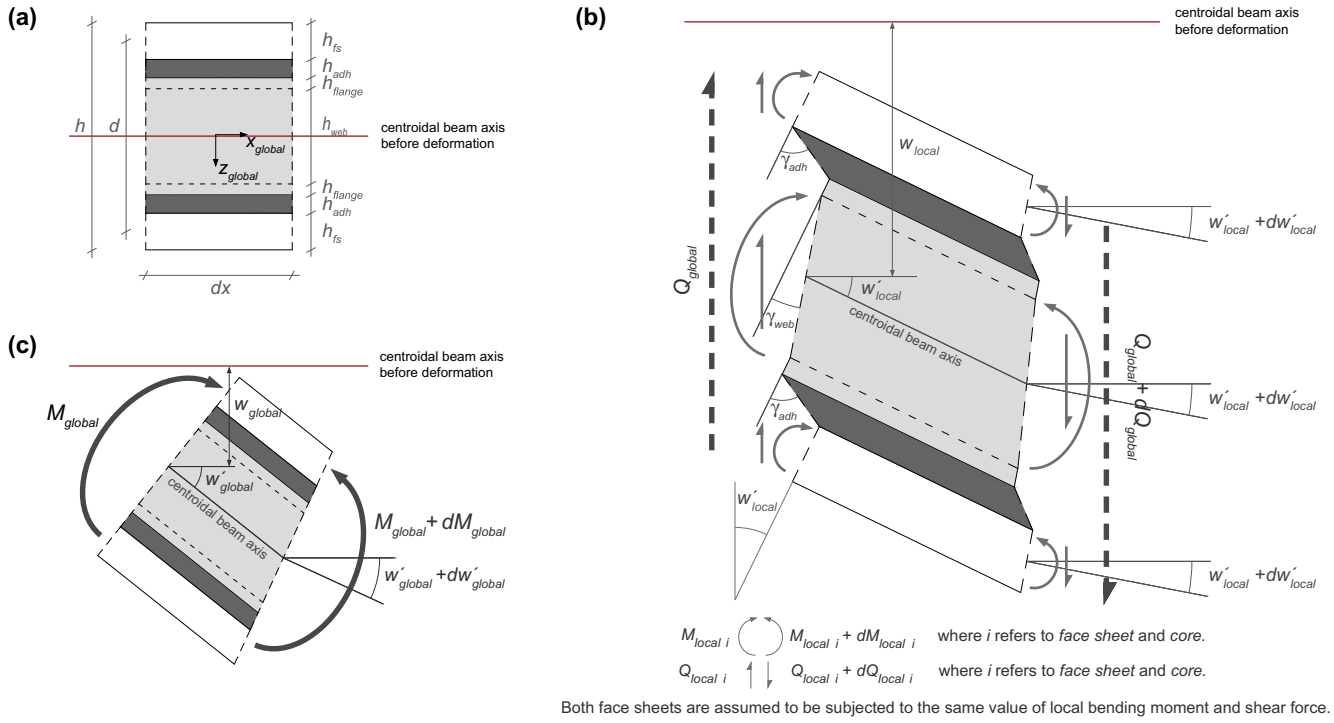

Fig. 4. Slice of a sandwich beam in three configurations: (a) undeformed configuration, and two deformed configurations produced by (b) local response and (c) global response.

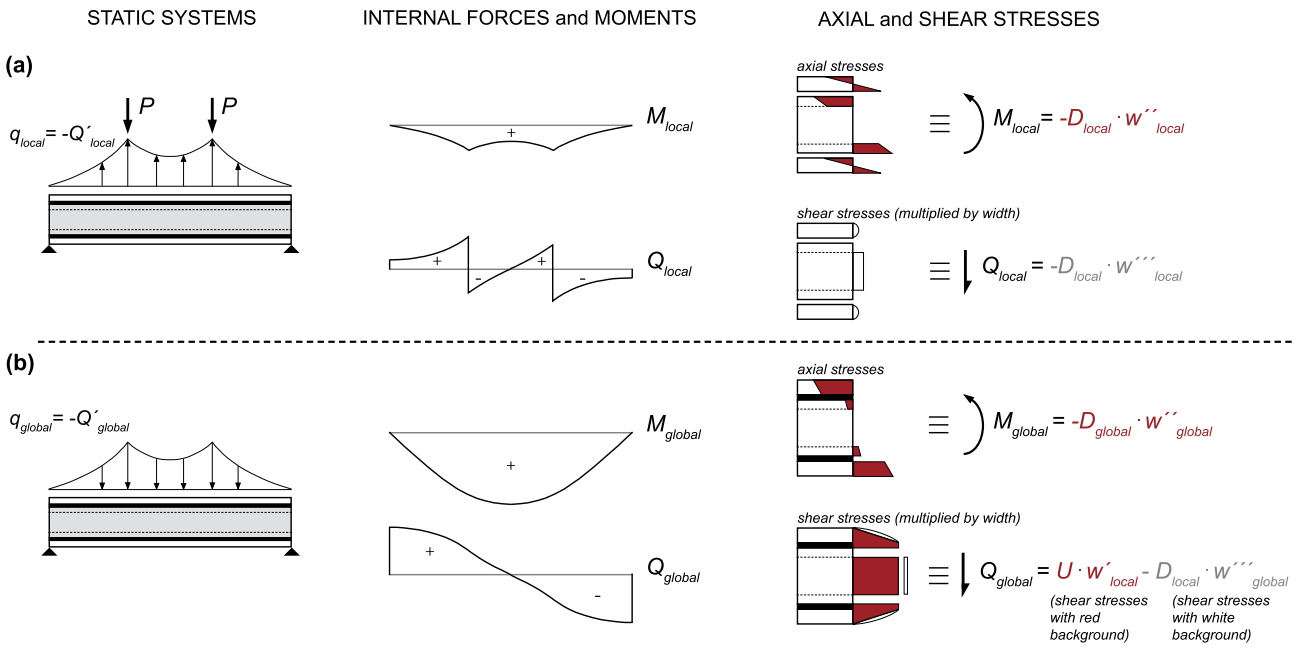

Fig. 5. Static systems, internal forces and bending moments, and axial and shear stresses produced by (a) local response and (b) global response.

D_{global}, of the sandwich structure depend on those of the constituent layers of the sandwich component according to:

$$D_{local} = (D_{local})_{top\ fs} + (D_{local})_{bottom\ fs} + (D_{local})_{core} \quad (1)$$

$$D_{global} = (D_{global})_{top\ fs} + (D_{global})_{bottom\ fs} + (D_{global})_{adh} + (D_{global})_{core} \quad (2)$$

where the corresponding local and global flexural rigidities of top face sheet (*top fs*), bottom face sheet (*bottom fs*), core (*core*) and adhesive (*adh*) layers are calculated as indicated in Eqs. (A.5) and (A.6) of the Appendix A. The cross-sectional shear stiffness, U, of adhesively-bonded sandwich structures results in:

$$U = G_{adh} \cdot A_{shear,sandwich} \quad (3)$$

where G_{adh} is the shear modulus of the adhesive and $A_{shear,sandwich}$ is the shear area of the sandwich structure given by Eq. (A.13).

2.4. Solutions of deflections and strains

The deflections are calculated based on the equation of equilibrium of shear forces (see Appendix Section A.3) as follows: 1) Q_{global} is obtained from Eq. (A.16) for the known distribution of Q_{total} shown in Fig. 3, and then substituted into Eq. (A.4) from where w_{global} is obtained and 2) Q_{local} is obtained from Eq. (A.14) and then substituted into Eq. (A.3) from where w_{local} is obtained. The solution for deflections associated with the global and local responses is given in the following for the regions *AB* (half the load span) and *BC* (shear span) of the system shown in Fig. 3d which is statically equivalent to that shown in Fig. 3a:

$$w_{global,equi\ AB} = \frac{-P}{D_{global}} \cdot \left(\frac{L_b}{2} \cdot X^2 + \frac{\mu_1}{a^3} \cdot (\cosh aX - 1) \right) \tag{4}$$

$$w_{local,equi\ AB} = \frac{-P}{D_{local}} \cdot \left(\frac{\mu_1}{a^3} \cdot (1 - \cosh aX) \right) \tag{5}$$

$$w_{global,equi\ BC} = \frac{-P}{D_{global}} \cdot \left(-\frac{X^3}{6} + \frac{L_b}{2} \cdot X^2 + \frac{L_a L_b a^2 - 1}{a^2} \cdot X + \frac{\mu_1}{a^3} \cdot (\cosh aX - 1) \cdot (\cosh aL_a) + \frac{\mu_2}{a^3} \cdot \sinh aX \right) \tag{6}$$

$$w_{local,equi\ BC} = \frac{-P}{D_{local}} \cdot \left(\frac{X}{a^2} + \frac{\mu_1}{a^3} \cdot (1 - \cosh aX) \cdot (\cosh aL_a) - \frac{\mu_2}{a^3} \cdot \sinh aX \right) \tag{7}$$

where coordinate X and deflections in each region (*AB* and *BC*) are given in the reference systems shown in Fig. 3d and coefficients μ_1 and μ_2 are given by:

$$\mu_1 = \frac{-\sinh aL_b}{\cosh a(L_a + L_b)} \tag{8}$$

$$\mu_2 = \frac{\cosh aL_a \cdot \cosh aL_b}{\cosh a(L_a + L_b)} \tag{9}$$

and a is a coefficient that depends exclusively on the flexural rigidities and shear stiffness of the sandwich component (see Eq. (A.15)). Axial strains in the sandwich component can be calculated analytically according to the curvatures produced by the local and global responses:

$$\varepsilon_{analyt} = -w''_{local} \cdot z_{local} - w''_{global} \cdot z_{global} \tag{10}$$

where the curvature w''_{local} is obtained by deriving Eqs. (5) and (7) (for regions *AB* and *BC* respectively), the curvature w''_{global} is obtained by deriving and Eqs. (4) and (6) (for regions *AB* and *BC* respectively) and z_{local} and z_{global} are the vertical coordinates of the coordinate systems shown in Fig. 1 – the origin of z_{local} changes for each constituent layer of the sandwich component and z_{local} and z_{global} superpose for the core. The shear strains in the adhesive layers can be calculated combining Eqs. (A.9) and (A.10) and results in:

$$\gamma_{analyt,adh} = \frac{w'_{local} \cdot d}{2 \cdot h_{adh} + \beta \cdot h_{web}} \tag{11}$$

where w'_{local} is obtained by deriving Eqs. (5) and (7) (for regions *AB* and *BC* respectively), h_{adh} and h_{web} are the thicknesses of adhesive layers and core-webs, d is the distance between face sheets centroids (Fig. 4) and coefficient β depends exclusively on the shear modulus and width of the adhesive layers and webs (Eq. (A.11)). The shear strains in the core-webs can be approximated as:

$$\gamma_{analyt,web} = \frac{w'_{local} \cdot d}{\frac{2}{\beta} \cdot h_{adh} + h_{web}} - \frac{(D_{local})_{core} \cdot w'''_{local}}{G_{web} \cdot b_{web} \cdot h_{web}} \tag{12}$$

where G_{web} and b_{web} are the shear modulus and width of the core-webs. The first term in the right hand side of Eq. (12) corresponds to the strains produced by Q_{global} (Eq. (A.10)) and the second term constitutes an approximation of the shear strains produced by Q_{local} (these strains are disregarded in the kinematics of Fig. 4b and in the analytical calculation of deflections and axial strains, see model assumptions) and corresponds to the ratio between the local shear force in the core-webs (numerator) and the product of the shear modulus and area of the core-webs (denominator).

2.5. Composite action in sandwich structures

The mid-span sandwich deflection (point *A*, see Fig. 3a) can be calculated from:

$$w_{analyt,A} = -(w_{global,equi\ B} + w_{local,equi\ B} + w_{global,equi\ C} + w_{local,equi\ C}) \tag{13}$$

where the deflections in the right-hand side are calculated with Eqs. (4) and (5) (for point *B*) and Eqs. (6) and (7) (for point *C*). For a sandwich structure with mid-span deflections $w_{analyt,A}$, the percentage of composite action, η, between face sheets and core can be defined in terms of deflections as:

$$\eta = \frac{w_{layered,A} - w_{analyt,A}}{w_{layered,A} - w_{monolithic,A}} \cdot 100\% \tag{14}$$

where $w_{layered,A}$ and $w_{monolithic,A}$ are respectively the mid-span sandwich deflections that would be obtained with Eq. (13) if very shear-flexible adhesives; i.e. $G_{adh} \to 0$ (layered structure), and shear-rigid adhesives, i.e. $G_{adh} \to \infty$ (monolithic structure), were employed. In fact, as shown in subsequent parts of this paper, G_{adh} = 2 GPa is sufficiently large to generate full composite action (i.e. monolithic limit is achieved).

3. Characterisation of polymeric materials for proposed sandwich concept

3.1. Sandwich beams and materials

Three sandwich beams were fabricated in this study with the proposed configuration shown in Fig. 1. The face sheets of these beams consist of fully toughened soda-lime-silica glass manufactured to BS EN 12150 [21] and measuring 150 × 500 × 10 mm^3. The sandwich cores were made of GFRP pultruded profiles produced by Exel Composites with a square-hollow section of dimensions 38 × 38 × 3 mm^3 and a length of 500 mm – the profile had a polyester matrix reinforced by E-glass fibres. The glass face sheets were bonded to the GFRP core with a 2-mm thickness adhesive layer made of the two-component structural epoxy DP490 from 3M – the two components of the adhesive were mixed in proportions 1.3 (*base*) to 1 (*accelerator*). These three beams were subsequently evaluated experimentally under four-point loads for a clear span L = 460 mm and their cross-section dimensions are indicated in Table 1. In the following text all beams, i.e. those described above (Fig. 1) and those investigated by Correia et al.[20] (Fig. 2), are labelled according to the core, adhesive and face sheet materials, i.e. GFRP-DP490-glass refers to the sandwich beam configuration shown in Fig. 1.

3.2. Burn-off experiment

In order to estimate the elastic and shear moduli of the GFRP core profiles, the fibre and resin volume fractions of five GFRP specimens were investigated by subjecting them to a burn-off experiment based on ASTM D3171-11 [22]. The specimens were cut from a 38 × 38 × 3 mm^3 square-hollow section core profile. Four

Table 1
Cross-section dimensions of the sandwich beams shown respectively in Figs. 1 and 2.

Sandwich beam	Core				Adhesive layers		Face sheets	
	Webs		Flanges					
	b_{web} (mm)	h_{web} (mm)	b_{flange} (mm)	h_{flange} (mm)	b_{adh} (mm)	h_{adh} (mm)	b_{fs} (mm)	h_{fs} (mm)
GFRP-DP490-glass	6	32	38	3	38	2	150	10
Glass-Sikadur330-GFRP[a]	12	100	–	–	76	2	76	10
Glass-Sikaflex260-GFRP[a]								

Note: [a]Two GFRP angle profiles ($30 \times 20 \times 4.8$ mm^3) strengthened the beams.

of these specimens were small-scale (SS) and had nominal dimensions $20 \times 30 \times 3$ mm^3 (specimens were cut one from each of the four sides of the profile) and one specimen was large-scale (LS) and corresponded to a 10-mm thick profile slice (Fig. 6). All the specimens were placed into ceramic crucibles and placed into a furnace for 5 h, with the following temperature profile: 1.5 h heating ramp from ambient temperature to 550 °C, 2 h at 550 °C and 1.5 h cooling ramp from 550 °C to ambient. The experiment revealed a three-layer fibre architecture in all the specimens: an inner layer made of unidirectional (UD) glass fibres and two outer layers made of chopped (mat) glass fibres (Fig. 6). The SS specimens were measured on weighing scales and showed that the UD and mat reinforcements constituted 73% and 27% of the total reinforcement weight, respectively.

The fibre volume fractions, V_f, of the five specimens were calculated from ASTM D3171-11 and the results are shown in Table 2 – for the calculations, fibre and resin densities were assumed as being 2.6 g·cm^{-3} and 1.2 g·cm^{-3} respectively [23]. In order to validate the results, the resin volume fractions, V_r, were also investigated based on ASTM D3171-11 from which the void volume fractions, V_v, were obtained as $V_v = 1 - V_f - V_r$ (Table 2). The void volume fractions were close to zero which is typical of pultruded profiles and confirmed that V_f and V_r were accurately estimated. The slightly higher value of the fibre volume fraction of the LS specimen (0.45) compared to the mean value of the SS specimens (0.43) was attributed to a higher fibre volume fraction in the corner regions of the profile.

The in-plane elastic and shear moduli of the UD and mat layers were calculated according to CUR96 [24]– assuming that for both layers $V_f = 0.43$ (mean value of the SS specimens) and the properties of fibres and matrix shown in Table 3. The elastic and shear moduli in the other planes were obtained directly from the in-plane values on the basis of the following assumptions: 1) mat layers are isotropic and 2) UD layers are transversally isotropic (i.e. isotropic in the unreinforced yz-plane – in this plane the shear modulus was assumed to be equal to that of the matrix). Finally the elastic and shear moduli of the webs and flanges of the pultruded GFRP profile were calculated as the weighted sum of the corresponding values multiplied by 0.73 or 0.27 for the UD and mat layers, respectively. The results are shown in Table 3. A basic validation of elastic (E_x) and shear (G_{xz}) moduli was performed by means of three-point-bending experiments on three nominally identical 200-mm span beams. The beams were loaded at a rate of 0.1 mm·min^{-1} with a 30-kN electromechanical testing machine (Instron 5567) and equipped at mid-span with a LVDT transducer (Fig. 7a). The results showed good agreement with the load-deflection response predicted by beam theory (including shear deformation in the webs) (Fig. 7b).

Table 2
Fibre volume fraction (V_f), resin volume fraction (V_r) and void volume fraction (V_v) of the four small-scale (SS) specimens and of the large-scale (LS) specimen subjected to burn-off experiment.

Specimen	V_f (–)	V_r (–)	V_v (–)
SS-1	0.47	0.55	−0.02
SS-2	0.44	0.56	0.00
SS-3	0.43	0.55	0.02
SS-4	0.39	0.59	0.02
LS	0.45	0.55	0.00
Mean (SS specimens)	0.43 ± 0.03	0.56 ± 0.02	0.01 ± 0.02

3.3. Single-lap shear experiments

The elastic and shear moduli of the DP490 adhesive were obtained from two single-lap shear specimens (SL-1 and SL-2) with two lap joints per specimen. The geometry of the specimens is shown in Fig. 8a and b. The specimens were fabricated with DP490 adhesive (mixture ratio 1.3:1 and bonded area of 50×25 mm^2), toughened glass plates (dimensions $200 \times 200 \times 10$ mm^3) and pultruded GFRP strips (made of polyester matrix and dimensions $95 \times 50 \times 6$ mm^3) – all materials and materials suppliers were identical to those in the GFRP-DP490-glass beams. The glass and GFRP surfaces were degreased with isopropyl alcohol prior to bonding. The assembly of the specimens was achieved using specially designed polytetrafluorethylene coated jigs which ensured a 2-mm bond thickness and correct alignment of the GFRP

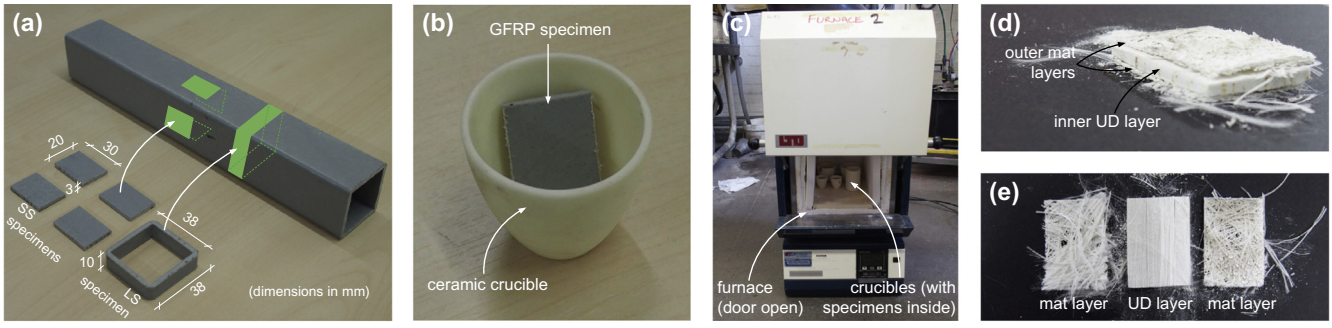

Fig. 6. (a) Specimens cut from pultruded GFRP profile for burn-off experiment, (b) specimen located into ceramic crucible, (c) crucibles introduced into furnace and (d–e) fibre architecture revealed after burn-off experiment.

Table 3
Material properties of matrix, fibres and GFRP layers together with those of GFRP-DP490-glass beam components for numerical models (values with shaded background) – all properties expressed in reference system shown in Fig. 1a.

Property	GFRP constituents		GFRP layers		GFRP webs and flanges	Adhesive	Glass face sheets
	Matrix[a]	Fibres[a]	UD layer	Mat layer			
E_x	3.4	72.0	31.9	11.9	26.5	$135 \cdot 10^{-3}$	72.0
E_y			9.2		9.9		
E_z (GPa)			9.2		9.9		
G_{xy}	1.2	29.5	2.8	3.7	3.0	$49 \cdot 10^{-3}$	29.5
G_{xz}			2.8		3.0		
G_{yz} (GPa)			1.2		1.9		

Note: [a]Properties obtained from Barbero (assumed identical for face sheets and fibres) [23].

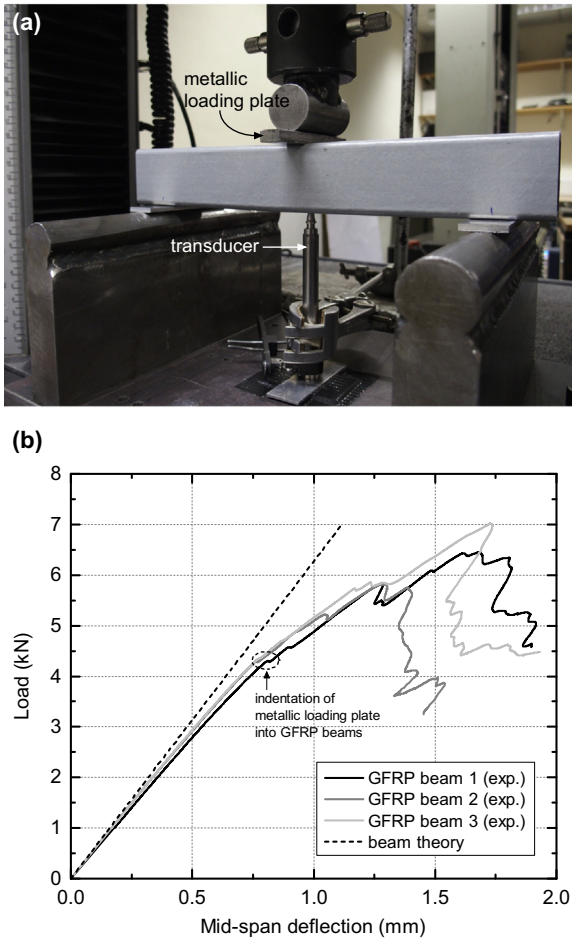

Fig. 7. (a) Three-point-bending experiment on 200-mm span GFRP beam and (b) applied load vs. mid-span deflection obtained experimentally and according to beam theory (shear deformation considered in the webs).

and glass plates. The two specimens were left to cure for seven days at ambient temperature. Single-lap shear experiments were then performed by means of a 150-kN electromechanical testing machine (Instron 5500R) pulling on the GFRP strips (Fig. 8c). The experiments were displacement controlled at a rate of 0.2 mm·min^{-1} up to failure and at ambient laboratory conditions (23 ± 3 °C and 50 ± 10% RH). The applied loads, P, on the specimens were measured by the load cell of the Instron machine and the relative displacement, Δl, between GFRP and glass components were measured with LVDT transducers fixed to the GFRP strips and resting against aluminium angles which were bonded to the glass plates (Fig. 8c) – Δl corresponded to the change in the reference length l indicated in Fig. 8a and was assumed to be produced only by the shear distortion of the adhesive bonds (deformations in the stiff GFRP and glass components were disregarded). Each specimen was equipped with two transducers, i.e. one transducer per lap joint.

The P-Δl curves obtained for the two specimens exhibited a linear response up to the failure which occurred due to glass fracture at ultimate loads, P_{ult}, of around 17 kN (Fig. 9). Assuming constant shear strains in the adhesive – as shown by Nhamoinesu [25] for similar structural joints –, the shear modulus of the adhesive in this single-lap configuration was calculated from:

$$G_{adh} = \frac{P_{ult}/A}{\Delta l / h_{adh}} \tag{15}$$

where A is the bonded area of the lap joint (1250 mm^2) and h_{adh} is the thickness of the adhesive (2 mm). An average value of G_{adh} = $(49 \pm 10) \cdot 10^{-3}$ GPa resulted from Eq. (15) and is reported in Table 3. Considering isotropy, the elastic modulus of the adhesive, E_{adh}, was calculated from:

$$E_{adh} = G_{adh} \cdot 2 \cdot (1 + \nu_{adh}) \tag{16}$$

where ν_{adh} is the Poisson's ratio of the adhesive (ν_{adh} = 0.38 according to Nhamoinesu [25]). From Eq. (16) an average value of E_{adh} = $(135 \pm 28) \cdot 10^{-3}$ GPa was obtained and is reported in Table 3. The relatively large standard deviations of the elastic and shear moduli amounted to approximately 20% of the corresponding mean value. This effect was attributed to the intrinsic material variability and extrinsic variability arising from manual dosing, mixing and specimen assembly.

4. Numerical validation and experimental investigation of new analytical models

4.1. Assessment of new models of flexural rigidities and shear stiffness

The newly developed analytical models given by Eqs. (1)–(3) were applied to the GFRP-DP490-glass beams (span-to-depth ratio of L/h = 7, L_a = 80 mm and L_b = 150 mm) and to the two adhesively-bonded beams tested by Correia et al. under four-point-bending loads [20] (cross section shown in Fig. 2, L/h = 12, L_a = 250 mm and L_b = 500 mm). The two latter beams were made of pultruded GFRP strip face sheets and annealed glass webs and differed in terms of the adhesives (Sikadur 330 and Sikaflex 265) used to bond face sheets and webs – these beams were labelled Glass-Sikadur330-GFRP and Glass-Sikaflex265-GFRP. The two following considerations were made: 1) the contributions of the four GFRP angle profiles (Fig. 2) to D_{local} and U were considered negligible

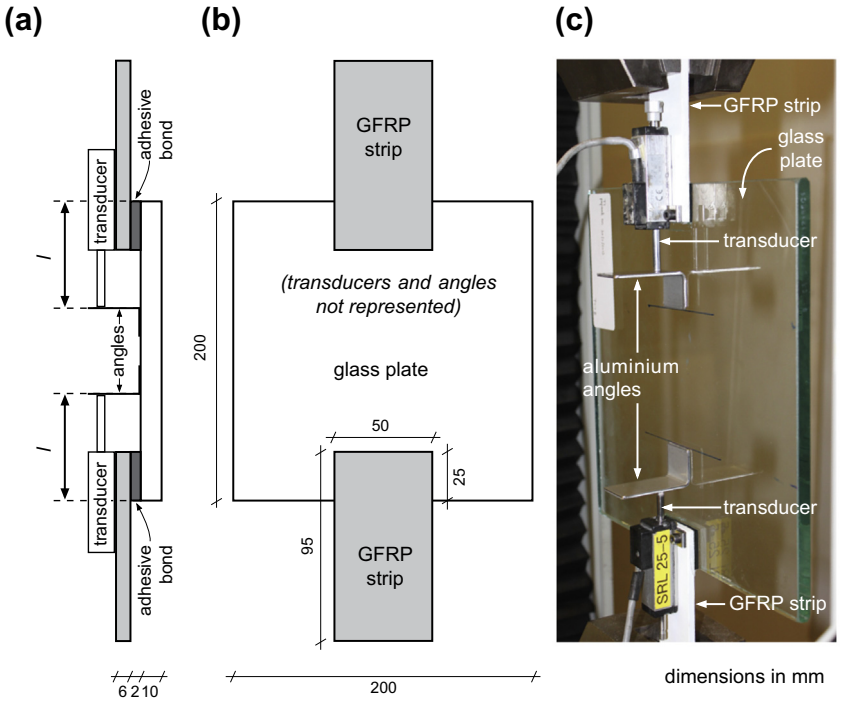

Fig. 8. Schematic (a) side view and (b) front view of single-lap shear specimens and (c) view of experimental set-up (not to scale).

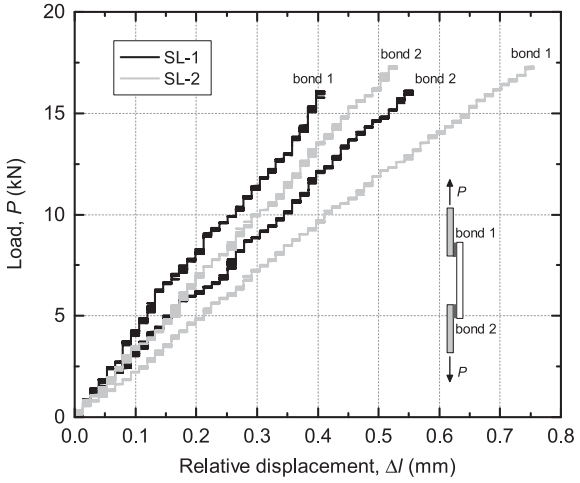

Fig. 9. Applied load vs. relative displacement of glass and GFRP substrates for the two single-lap shear (SL) specimens.

and 2) the contributions of the thick (glass) core-webs to D_{local} and D_{global} were considered non-negligible and included in the calculations. Cross section dimensions of all beams are given in Table 1 and material properties for analytical models are given in Table 4. The resulting global flexural rigidities (D_{global}), local flexural rigidities (D_{local}) and shear stiffnesses (U) are reported in Table 5. The GFRP-DP490-glass beams exhibited the highest value of D_{global} indicating that the configuration of these beams was more suitable for resisting bending – the stiffer material (glass) employed for the face sheets and the softer material (GFRP) for the core. However these beams had the lowest local flexural rigidity due essentially to the very low height of their core profile. The shear stiffnesses of the beams were significantly affected by the shear modulus of the adhesives: beams bonded with stiffer adhesives had higher shear stiffness.

4.2. Numerical validation

A three-dimensional (3D) finite element model of the four-point bending experiments performed on the GFRP-DP490-glass beams ($L/h = 7$) was developed using Ansys Mechanical APDL v16.2 software – the experiments are presented below. Eight further finite element models were simulated for beams with identical cross-section dimensions, material properties and loading configuration (i.e. L_a/L_b) to the GFRP-DP490-glass beams but with L/h of 8, 9, 10, 11, 12, 16, 20 and 40. The beams are bi-symmetric, therefore only one quarter of the beams were modelled (Fig. 10). The material properties adopted for the numerical analyses are indicated in Table 3 – all materials were assumed linear elastic and a perfect bonding was assumed. A mapped orthogonal mesh of SOLID45 elements – cubic elements with eight nodes per element (one per vertex) and three degrees of freedom (three displacements along

Table 4
Material properties for analytical models of flexural rigidities and shear stiffness.

Sandwich beam	GFRP		Adhesive		Glass	
	E (GPa)	G (GPa)	E (GPa)	G (GPa)	E (GPa)	G (GPa)
GFRP-DP490-glass	26.5	3.0	$135 \cdot 10^{-3}$	$49 \cdot 10^{-3}$	72	29.5
Glass-Sikadur330-GFRP[a]	32 (face sheets)	3.6	5.1	1.9	72	29.5
Glass-Sikaflex265-GFRP[a]	19.7 (angles)	3.6	$1.5 \cdot 10^{-3}$	$0.5 \cdot 10^{-3}$	72	29.5

Note: [a]Properties of GFRP and adhesive obtained from Correia et al. [20].

Table 5
Span-to-depth ratio, spans, global and local flexural rigidities and shear stiffness of investigated sandwich beams.

Sandwich beam	L/h (–)	L (mm)	L_a (mm)	L_b (mm)	D_{global} (N·mm^2)	D_{local} (N·mm^2)	U (N)
GFRP-DP490-glass	7	460	80	150	$1.50 \cdot 10^{11}$	$3.65 \cdot 10^{9}$	$6.09 \cdot 10^{5}$
Glass-Sikadur330-GFRP	12	1500	250	500	$2.70 \cdot 10^{10}$	$7.24 \cdot 10^{10}$	$4.19 \cdot 10^{7}$
Glass-Sikaflex265-GFRP	12	1500	250	500	$2.64 \cdot 10^{10}$	$7.24 \cdot 10^{10}$	$1.23 \cdot 10^{5}$

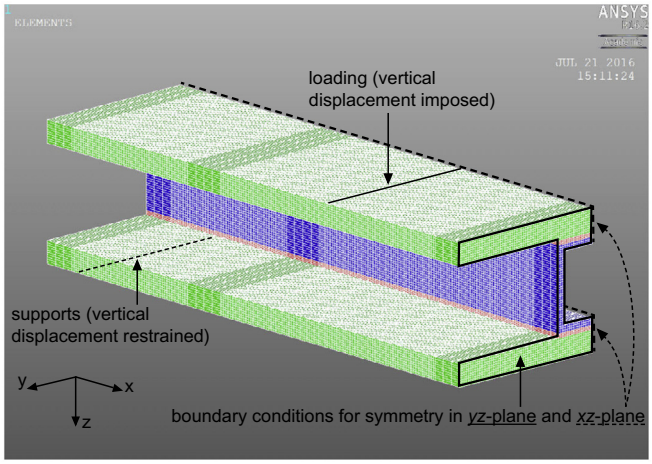

Fig. 10. Geometry, mesh and boundary conditions considered for finite element model of GFRP-DP490-glass sandwich beam subjected to four-point bending loads.

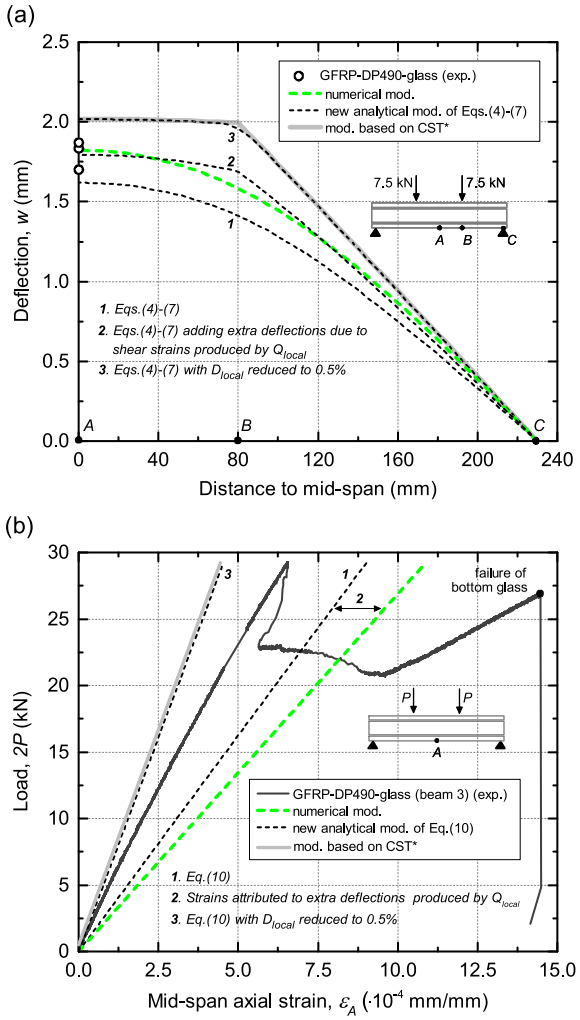

Fig. 11. Analytical, numerical and experimental (a) deflections and (b) mid-span axial strains in GFRP-DP490-glass beams. Note: *CST refers to classical sandwich theory (it disregards local bending moments) [18].

Cartesian axes) at each node – was used for all the beams modelled as follows: the through-thickness z-direction was meshed with 1-mm size elements in the glass and GFRP components and 0.5-mm size elements in the adhesive layers. For the x- and y-directions 1-mm mesh size elements were initially selected. In the beam with $L/h = 7$ a sensitivity analysis showed that increasing the mesh size to 5 mm in the x-direction for elements further away from the applied loads had no influence on the numerical results (i.e. deflections, axial and shear strains and reactions) and therefore this meshing was selected for all the beams in order to reduce computational time. For the GFRP-DP490-glass beams ($L/h = 7$), the percent discrepancies of analytical predictions with respect to numerical predictions were small: −11% for mid-span deflections (calculated with Eqs. (4)–(7)) and 18% for mid-span axial strains on lower surface of bottom face sheet (calculated with Eq. (10)) (Fig. 11). The discrepancies are reported in Table 6 (mid-span deflections, w_A) and Table 7 (mid-span axial strains, ε_A). Moreover for increasing values of L/h percent discrepancies between analytical and numerical methods reduced rapidly and converged to approximately 0% (for mid-span deflections and axial strains) and 10% (for shear strains at mid-span of shear span BC) for $L/h = 40$ (Fig. 12).

4.3. Experimental investigation

The three 460-mm span GFRP-DP490-glass beams were evaluated under four-point bending loads up to failure. The loads were applied on the beams by means of a 150-kN electromechanical testing machine (Instron 5500R) connected to a metallic distribution frame which included two steel rollers at a distance of 160 mm (Fig. 13a and b). The testing machine was connected with a hinge to the top of the distribution frame to ensure symmetric loading. The experiments were displacement controlled at a rate of 0.25 mm·min^{-1} and at ambient laboratory conditions (23 ± 5 °C and 50 ± 10% RH). The applied loads, $2P$, were measured by the 150-kN load cell fitted in the Instron machine, where P represents the load transmitted by each steel roller to the beam. The mid-span deflections, w_A, of the three sandwich beams were measured with a LVDT transducer located below the bottom glass face sheet (Fig. 13a). For one sandwich beam, a unidirectional strain gage (TML, FLA-6-11) was bonded at mid-span on the bottom face sheet surface to measure the axial strains, ε_A, in the glass (Fig. 13a). The three $2P$-w_A experimental curves are shown in Fig. 14. The response is almost linear up to the longitudinal shear failure of the pultruded core profiles (close to the supports as shown in Fig. 13c) that occurred at loads between 20 kN and 30 kN and at mid-span deflections of around 3 mm. The shear failure of the cores produced a reduction in the resisted loads. The loads subsequently increased on a reduced stiffness path to around 27 kN and the bottom glass face sheet, subjected to the highest tension stresses, fractured (Fig. 13d). Then the resisted loads reduced. As the loads subsequently increased on a significantly reduced stiffness

Table 6
Comparison between numerically, analytically and experimentally obtained mid-span deflections.

Sandwich beam	L/h (–)	$2P$ (kN)	Numerical $w_{num,A}$ (mm)	Analytical $w_{analyt,A}$ (mm)	Experimental $w_{exp,A}$ (mm)	$\Delta w_{analyt\text{-}num,A}$ (%)	$\Delta w_{analyt\text{-}exp,A}$ (%)
GFRP-DP490-glass	7	15	1.8	1.6	1.8 (mean value)	−11	−11
Glass-Sikadur330-GFRP	12	15	–	3.4	3.4[a]	–	0
Glass-Sikaflex265-GFRP	12	4.5	–	2.8	2.7	–	4

Note: [a]Values from Correia et al. [20].

Table 7
Comparison between numerically, analytically and experimentally obtained mid-span axial strains on lower surface of bottom face sheet.

Sandwich beam	L/h (–)	$2P$ (kN)	Numerical $\varepsilon_{num,A}$ ($\cdot 10^{-4}$) (–)	Analytical $\varepsilon_{analyt,A}$ ($\cdot 10^{-4}$) (–)	Experimental $\varepsilon_{exp,A}$ ($\cdot 10^{-4}$) (-)	$\Delta\varepsilon_{analyt\text{-}num,A}$ (%)	$\Delta\varepsilon_{analyt\text{-}exp,A}$ (%)
GFRP-DP490-glass	7	15	5.6	4.6	3.1	-18	48
Glass-Sikadur330-GFRP	12	15	–	8.6	6.8[a]	–	26
Glass-Sikaflex265-GFRP	12	4.5	–	1.5	1.0[a]	–	50

Note: [a]Values from Correia et al. [20].

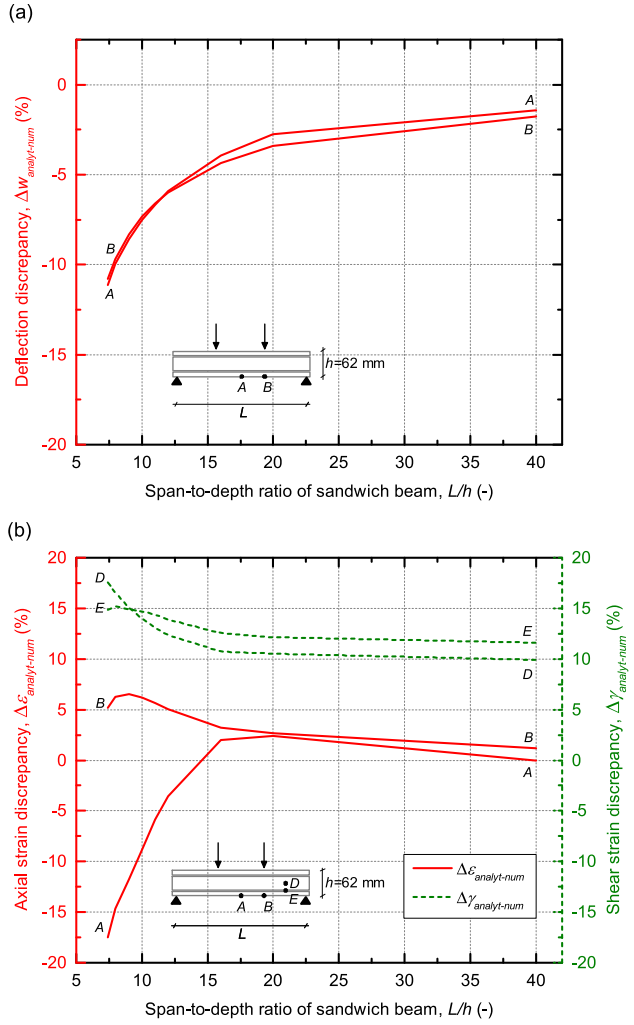

Fig. 12. Percent discrepancies of analytical predictions with respect to numerical predictions of (a) deflections and (b) axial and shear strains as a function of span-to-depth ratio of sandwich beams. Note: points D and E are located at mid-span of the shear-span BC in the centre of core-webs and in adhesive layer respectively – in the numerical models shear strain in point E was considered as the average strain of all the nodes in the same adhesive cross-section.

path up to around 15 kN, the top glass face sheet fractured (Fig. 13e). In the initial linear range of the curves the experimental $2P$–w_A results were in very good agreement with the analytical predictions (Fig. 15) and percent discrepancy of analytical predictions with respect to average experimental results was only of −11% (Table 6). However analytical predictions significantly overestimated the experimental mid-span axial strains – at $2P = 15$ kN, the analytical prediction exceeded by 48% the experimental result (Fig. 11b and Table 7).

The $2P$-w_A experimental curves of the Glass-Sikadur330-GFRP and Glass-Sikaflex265-GFRP beams tested by Correia et al. are shown in Fig. 16 [20]. The responses of the beams were almost linear up to the failure of the glass webs that occurred at load-displacement values of around 5 kN-3 mm (Glass-Sikaflex265-GFRP) and 26 kN-6.5 mm (Glass-Sikadur330-GFRP) – the post-fracture responses are omitted from Fig. 16 for clarity (details are given in Correia's work [20]). The $2P$-w_A curves obtained analytically provided a close prediction of the experimental results (Fig. 16 and Table 6). However, as for the beams presented above, the analytical predictions of mid-span axial strain (on lower surface of bottom face sheet) significantly overestimated the experimental results (Table 7): percent discrepancies were of 26% (Glass-Sikadur330-GFRP) and 50% (Glass-Sikaflex265-GFRP) – the larger discrepancy in the latter beam is associated to the very small values of experimental strains resulting in a high sensitivity of percent discrepancy to even small strain mismatches.

5. Discussion

On the contrary to classical sandwich theory that neglects the local flexural rigidity, the new equations for deflections (Eqs. (4)–(7)) and axial strains (Eq. (10)) developed in this work produce similar results than finite element analysis (see curves 1 in Fig. 11a and b). A closer matching of deflections was obtained for curve 2 (Fig. 11a) that considers the extra deflections resulting from integrating along the beam axis the shear strains produced by the local shear force (i.e. second term in the right-hand side of Eq. (12)). It has to be noticed that face sheets would participate in this extra deflections by bending about their own centroidal axes producing therefore additional axial strains (see Fig. 11b).

To investigate the influence of the local flexural rigidity on the results of the new equations of deflections and axial strains, D_{local} was reduced there to 0.5% of its original value and two effects were observed (see curves 3 in Fig. 11a and b): 1) results matched the predictions of classical sandwich theory, and 2) the mid-span axial strains reduced significantly and became lower than the experimental strains, with an only small increase of mid-span deflections. Therefore, the effect of D_{local} on the results of the new

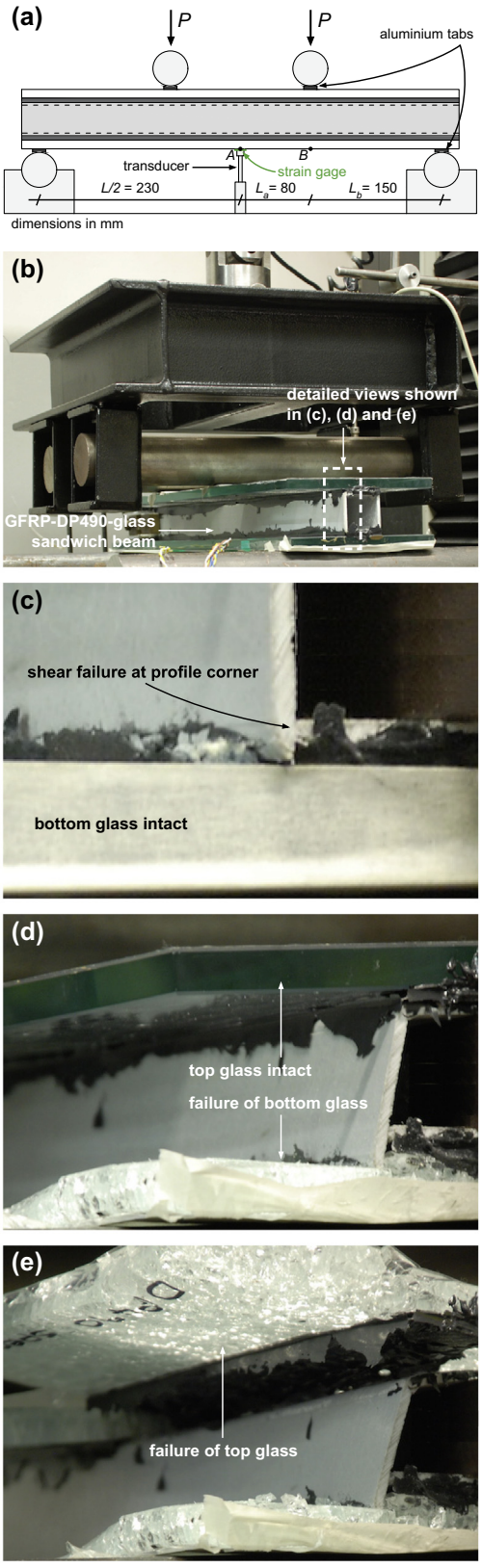

Fig. 13. (a) Schematic view of the four-point bending experimental set-up, (b) experiment performed on GFRP-DP490-glass beam and detailed views of the failure of (c) pultruded GFRP core profile, (d) bottom glass face sheet and (e) top glass face sheet.

equations of deflections is relatively small compared to that on axial strains and therefore the discrepancies of experimental strains vs. analytical (and numerical) strains in the GFRP-DP490-

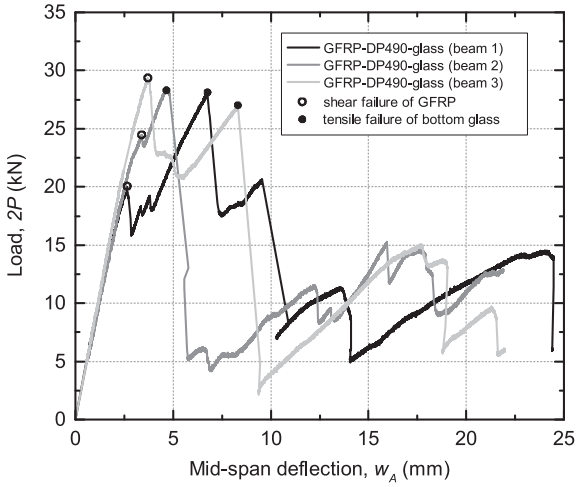

Fig. 14. Applied load vs. mid-span deflection measured experimentally for GFRP-DP490-glass beams.

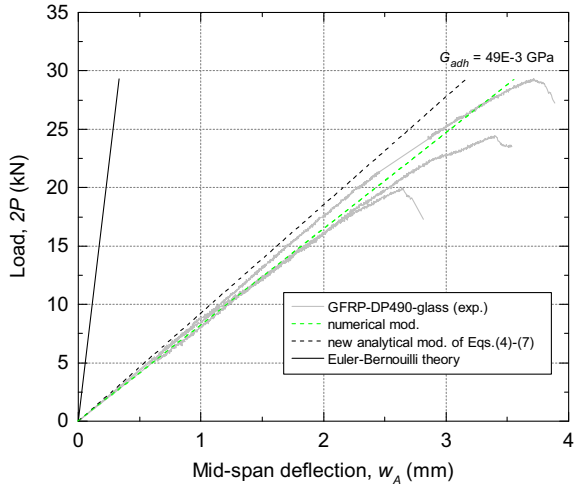

Fig. 15. Applied load vs. mid-span deflection obtained analytically, numerically and experimentally for GFRP-DP490-glass beams (experimental curves are shown up to GFRP failure).

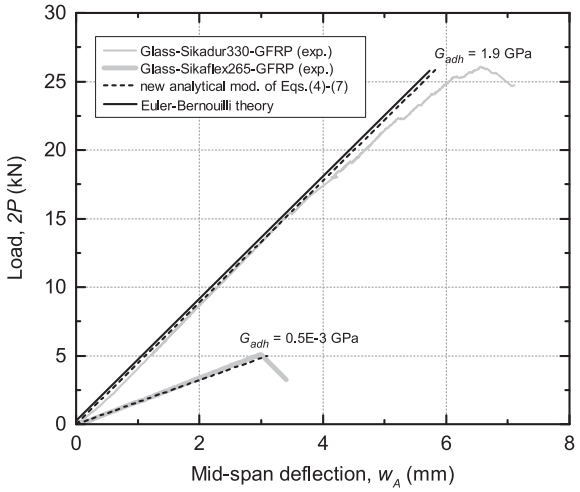

Fig. 16. Applied load vs. mid-span deflection obtained analytically and experimentally (by Correia et al. [20]) for Glass-Sikaflex265-GFRP and Glass-Sikadur330-GFRP beams (post-fracture response of beams not represented).

glass beam (see Table 7) are likely to be caused by less local bending effects at the mid-span of the tested beam than those resulting from the new analytical models. This may be due to an imperfect bonding between face sheets and core (e.g. non-constant adhesion along the bonded surfaces, debondings and/or delaminations) not considered by the analytical and numerical models. Further experimental investigation of the local bending moments, deflections and strain distribution has to be performed in adhesively-bonded sandwich components monitored with more LVDT transducers and strain gages (e.g. bonded on top and bottom surfaces of each face sheet to capture the effects of the local bending moments).

A comparison is made for the mid-span deflections resulting from the new analytical models, $w_{analyt,A}$, and by ordinary Euler-Bernoulli bending theory, $w_{EB,A}$, for beams with the cross-sections shown in Figs. 1 and 2. To this purpose the ratio of deflections $w_{analyt,A}/w_{EB,A}$ has been investigated as a function of the shear modulus of the adhesive and span-to-depth ratio of sandwich beams and the results are shown in Fig. 17. The predictions of ordinary bending theory and those of the new analytical models match for sandwich beams with shear-stiff cores (i.e. glass cores) and relatively stiff adhesives ($G_{adh} > 0.1$ GPa), i.e. structures with negligible shear deformations (Figs. 16 and 17). For sandwich components with shear-flexible adhesives or cores (e.g. GFRP-DP490-glass and Glass-Sikaflex265-GFRP beams) ordinary bending theory largely underestimates the deflections especially for low span-to-depth ratios (Figs. 15–17). It can also be observed that an adhesive with a shear modulus of around $G_{adh} = 2$ GPa is sufficient to provide full composite action between face sheets and core. For the proposed GFRP-glass sandwich structures, the load-displacement responses and percentage of composite actions of four beams – $L/h = 12$, cross-section shown in Fig. 1b, material properties of glass and GFRP given in first row of Table 4 and G_{adh} ranging from 0 GPa (layered beam) to 2 GPa (monolithic beam) – were calculated according to Eqs. (4)–(7) and (14) and the results are shown in Fig. 18. Significantly stiffer structures can be obtained by using moderately stiff adhesives (G_{adh} = 49E−3 GPa, e.g. DP490 adhesive) than those obtained with low stiffness adhesives (G_{adh} = 0.5E−3 GPa, e.g. Sikaflex265 or structural silicones): the former adhesives allow for a composite action $\eta = 95\%$ (i.e. close to the monolithic beam response) whereas the latter adhesives result in $\eta = 16\%$ (i.e. only slightly stiffer than the layered beam response) – these values would increase for increasing span-to-depth ratios (e.g. for $L/h = 20$ the softer adhesive would allow for $\eta = 34\%$).

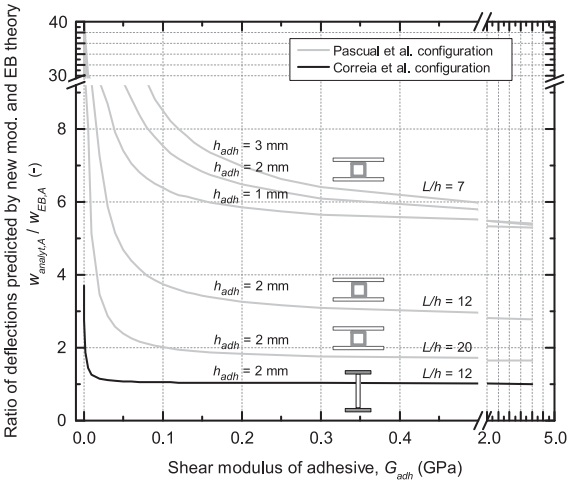

Fig. 17. Ratio of mid-span deflections predicted based on new analytical models and by ordinary Euler-Bernoulli bending theory vs. shear modulus of adhesive for two adhesively-bonded sandwich configurations.

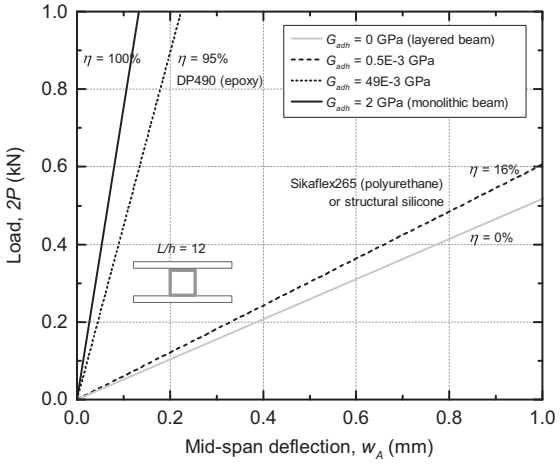

Fig. 18. Applied load vs. mid-span deflection predicted analytically for the proposed concept of GFRP-glass sandwich beams bonded with four different adhesives ($L/h = 12$ and $h_{adh} = 2$ mm).

Future work in relation with adhesively-bonded GFRP-glass sandwich structures concerns the study of the distribution of strains in the constituent layers, the study of the shear lag in the face sheets of large sandwich panels and the investigation of the structural response of these structures subjected to compressive loads, dynamic loads and long-term effects (thermal cycles and solar radiation).

6. Conclusions

The bending and shear response of adhesively-bonded GFRP-glass sandwich structures has been investigated and the following conclusions were drawn:

1. The feasibility of fabricating sandwich structures made of tempered glass thick face sheets adhesively-bonded to GFRP pultruded core profiles has been analytically, numerically and experimentally demonstrated. The proposed GFRP-glass sandwich concept offers potential for designing transparent, thin and structurally stiff building envelopes that outperforms existing non-composite envelope systems.
2. New analytical models for predicting the deflections and axial and shear strains of adhesively-bonded sandwich structures with shear-flexible adhesives and cores have been developed. The models have been validated by linear elastic numerical simulations and discrepancies between analytical and numerical predictions were only of around 11% (deflections) and 18% (axial and shear strains) for a span-to-depth ratio of 7 and reduced rapidly for larger ratios.
3. The analytical prediction of deflections has also been validated experimentally: analytical prediction underestimated experimental results by only 11%. However analytical prediction of mid-span axial strain (on lower face sheet) overestimated the experimental result by 48%. In contrast to deflections, axial strains appear to be very sensitive to the bending of face sheets about their own local axes. Further investigation of the strain distribution in sandwich structures is therefore required.
4. A composite action of 95% (in terms of deflections) can be obtained in the proposed GFRP-glass sandwich beams bonded with moderately stiff adhesives (G_{adh} = 49E−3 GPa) for a span-to-depth ratio of 12. This percentage of composite action is significantly higher than that provided by low shear modulus adhesives (G_{adh} = 0.5E−3 GPa), e.g. structural silicones, which has been predicted to be of 16%.

Acknowledgements

The authors would like to thank the Engineering and Physical Sciences Research Council – United Kingdom for the financial support of the project (grant number EP/MO 17699/1), Exel Composites for providing GFRP pultruded components, Prof. João R. Correia and Dr. Luís Valarinho for providing experimental data related to the Glass-Sikadur330-GFRP and Glass-Sikaflex265-GFRP beams and Susan Benson for her contribution to the experimental work performed in this research.

Appendix A. Derivation of analytical models

A.1. Models of sandwich flexural rigidities

Total, global and local bending moments and shear forces in the sandwich component are related by:

$$M_{total} = M_{local} + M_{global} \tag{A.1}$$

$$Q_{total} = Q_{local} + Q_{global} \tag{A.2}$$

The local and global flexural rigidities, respectively D_{local} and D_{global}, are related to the local and global shear forces and bending moments according to ordinary Euler-Bernoulli bending theory [15]:

$$Q_{local} = M'_{local} = -D_{local} \cdot w'''_{local} \tag{A.3}$$

$$Q_{global} = M'_{global} = -D_{global} \cdot w'''_{global} \tag{A.4}$$

where prime symbols indicate derivatives with respect to x-direction (derivatives of shear forces are distributed loads as shown in Fig. 5, which globally equate to zero). The local and global flexural rigidities, D_{local} and D_{global}, are calculated as the sum of the corresponding local and global flexural rigidities of the constituent layers given by:

$$(D_{local})_i = E_i \cdot \int_{A_i} z^2_{local_i} \cdot dA_i \tag{A.5}$$

$$(D_{global})_i = E_i \cdot \int_{A_i} z^2_{global} \cdot dA_i \tag{A.6}$$

where i refers to each constituent layer in the sandwich component (i.e. top face sheet, bottom face sheet, core and adhesive layers), E_i and dA_i are the elastic modulus and differential of cross-sectional area of the i-constituent layer and z_{local} and z_{global} are the vertical coordinates of local and global coordinate systems shown in Fig. 1 (both systems superpose for the core).

A.2. Model of sandwich shear stiffness

The global shear force, Q_{global}, is related to the shear stiffness, U, of the sandwich component by [15]:

$$Q_{global} = U \cdot w'_{local} - D_{local} \cdot w'''_{global} \tag{A.7}$$

where the contributions of $U{\cdot}w'_{local}$ and $-D_{local}{\cdot}w'''_{global}$ to the global shear force are shown in Fig. 5. The shear force $U{\cdot}w'_{local}$ produces a trapezoidal distribution in the sandwich cross-section of the product of shear stresses and width: constant in the core and adhesive layers and varying linearly to zero across the thickness of each face sheet – no shear lag is assumed, i.e. shear stresses are assumed constant at a given coordinate z_{global} (coordinate system shown in Fig. 1b). Therefore the term $U{\cdot}w'_{local}$ in Eq. (A.7) can be expressed as:

$$U \cdot w'_{local} = G_{adh} \cdot \gamma_{adh} \cdot b_{adh} \cdot (2 \cdot h_{adh} + h_{web} + h_{fs}) \tag{A.8}$$

where G_{adh}, γ_{adh}, b_{adh} and h_{adh} are the shear modulus, shear strain, width and thickness of the adhesive layers, respectively and h_{web} and h_{fs} are the thickness of core-webs and face sheets, respectively (Figs. 1 and 4) wherein the contribution of core-flanges to the shear stiffness has been disregarded. The shear strains in the adhesive layers, γ_{adh}, and core-webs, γ_{web}, are geometrically related to the slope w'_{local} of the global centroidal axis by (Fig. 4b):

$$w'_{local} = \frac{2 \cdot \gamma_{adh} \cdot h_{adh} + \gamma_{web} \cdot h_{web}}{d} \tag{A.9}$$

where d the is the distance between the centroids of glass face sheets (Fig. 4a). The shear strains in core-webs, γ_{web}, and adhesive layers, γ_{adh}, are assumed to be produced only by total shear forces Q_{global} – and particularly by the trapezoidal distribution of stresses described above (Fig. 5) –, therefore:

$$\gamma_{web} = \gamma_{adh} \cdot \beta \tag{A.10}$$

where coefficient β is given by:

$$\beta = \frac{G_{adh} \cdot b_{adh}}{G_{web} \cdot b_{web}} \tag{A.11}$$

where G_{web} and b_{web} are the shear modulus and width of core-webs, respectively (Fig. 1). Substituting Eq. (A.10) into Eq. (A.9), and then this one into Eq. (A.8), allows to obtain the cross-sectional shear stiffness, U, of adhesively-bonded sandwich structures given by:

$$U = G_{adh} \cdot A_{shear,sandwich} \tag{A.12}$$

where $A_{shear,sandwich}$ is the shear area of the sandwich structure and is calculated as:

$$A_{shear,sandwich} = \frac{d \cdot b_{adh} \cdot (2 \cdot h_{adh} + h_{web} + h_{fs})}{2 \cdot h_{adh} + \beta \cdot h_{web}} \tag{A.13}$$

where β is given by Eq. (A.11), d the is the distance between the centroids of glass face sheets, h_{adh}, h_{web} and h_{fs} are the thicknesses of adhesive layers, core-webs and face sheets respectively and b_{adh} is the width of the adhesive layers (Fig. 1).

A.3. Equation of equilibrium of shear forces

From Eqs. (A.4) and (A.7) an expression can be obtained for w'_{local} as a function of D_{global}, D_{local}, U and Q_{global} and substituting it into Eq. (A.3) gives the following relation between Q_{local} and Q_{global}:

$$Q_{local} = -\frac{1}{a^2} \cdot Q''_{global} \tag{A.14}$$

where a^2 depends exclusively on the flexural rigidities and shear stiffness of the sandwich component and is given by:

$$a^2 = \frac{U}{D_{local} \cdot \left(1 - \frac{D_{local}}{D_{global}}\right)} \tag{A.15}$$

Substituting Eq. (A.14) into Eq. (A.2) results in the following differential equation for sandwich structures subjected to transverse loads in static equilibrium:

$$Q_{total} = Q_{global} - \frac{1}{a^2} \cdot Q''_{global} \tag{A.16}$$

When $G_{adh} \to 0$ both U and $a^2 \to 0$ (see Eqs. (A.12) and (A.15)), therefore Eqs. (A.14) and (A.16) converge which correctly means that $Q_{total} \to Q_{local}$ and the performance of the sandwich structure converges to the layered limit (i.e. sandwich structure with unbonded layers).

Appendix B. Notation

b_i	width of constituent layer i
d	distance between face sheets centroids
D_{local}	local flexural rigidity of sandwich structure
D_{global}	global flexural rigidity of sandwich structure
E_i	elastic modulus of constituent layer i
G_i	shear modulus of constituent layer i
h_i	thickness of constituent layer i
M_{local}	local bending moment
M_{global}	global bending moment
Q_{local}	local shear force
Q_{global}	global shear force
U	shear stiffness of sandwich structure
w_{local}	deflection produced by local response
w_{global}	deflection produced by global response
$(z_{local})_i$	vertical coordinate of local reference system in constituent layer i
z_{global}	vertical coordinate of global reference system
ε	axial strain
γ	shear strain
η	percentage of composite action (in terms of deflections)

Appendix C. Supplementary data

Supplementary data associated with this article can be found, in the online version, at http://dx.doi.org/10.1016/j.compstruct.2016.10.059.

References

[1] Biggs R. Experiences with structural sandwich in building construction. In: Proceedings of symposium on durability and weathering of structural sandwich constructions, San Francisco, CA, 13 October 1959. p. 68–1.

[2] Engelsmann S, Spalding V, Peters S. Plastics. In: Architecture and construction. Basel: Birkhauser; 2010.

[3] Keller T, Haas C, Vallée T. Structural concept, design, and experimental verification of a glass fiber-reinforced polymer sandwich roof structure. J Compos Constr 2008;12(4):454–68.

[4] Knippers J, Cremers J, Gabler M, Lienhard J. Construction manual for polymers + membranes. Basel: Birkhauser; 2011.

[5] Palumbo D, Palumbo M, Mazzucchelli M. A new roof for the XIIIth Century "Loggia de Vicari" (Arqua Petrarca – PD – Italy) based on structural glass trusses: a case study. In: Proceedings of glass processing days, Tampere, 17–20 June 2005. p. 434–35.

[6] Louter C. High-strength fibre rods as embedded reinforcement in SentryGlas-laminated glass beams. In: Proceedings of glass performance days, Tampere, 12–15 June 2009. p. 285–89.

[7] Louter C, Leung C, Kolstein H, Vambersky J. Structural glass beams with embedded glass fibre reinforcement. In: Proceedings of challenging glass 2, Delft, 20–21 May 2010. p. 439–48.

[8] Wurm J. Glass structures: design and construction of self-supporting skins. Basel: Birkhauser; 2007.

[9] Peters S. Kleben von GFK und Glas fur baukonstruktive Anwendungen [PhD Thesis]. Germany: Universitat Stuttgart; 2006.

[10] Santarsiero M, Louter C, Nussbaumer A. The mechanical behaviour of SentryGlas ionomer and TSSA silicon bulk materials at different temperatures and strain rates under uniaxial tensile stress state. Glass Struct Eng 2016. http://dx.doi.org/10.1007/s40940-016-0018-1.

[11] Tomasi A, Mocibob D, van de Linde B, Wellershoff F, Koldtoft K. Tec facade – glass as functional façade element. In: Proceedings of COST action TU0905 mid-term conference on structural glass, Porec, 18–19 April 2013. p. 349–57.

[12] Overend M, Nhamoinesu S, Watson J. Structural performance of bolted connections and adhesively bonded joints in glass structures. J Struct Eng 2012;139(12):04013015.

[13] Laufs W, Sedlacek G. Stress distribution in thermally tempered glass panes near the edges, corners and holes. Part 2. Distribution of thermal stresses. Glass Sci Technol 1999;72(2):42–8.

[14] Nielsen J, Olesen J, Poulsen P, Stang H. Simulation of residual stresses at holes in tempered glass: a parametric study. Mater Struct 2010;43(7):947–61.

[15] Allen H. Analysis and design of structural sandwich panels. Oxford: Pergamon Press; 1969.

[16] Natterer J, Hoeft M. Zum tragverhaltra von holz – beton – verbundkonstructionen. Switzerland: Ecole Polytechnique Fédérale de Lausanne; 1987. Technical report CERS Nº 1345.

[17] Osei-Antwi M, de Castro J, Vassilopoulos A, Keller T. Modeling of axial and shear stresses in multilayer sandwich beams with stiff core layers. Compos Struct 2014;116(1):453–60.

[18] Zenkert D. An introduction to sandwich construction. Warrington: Engineering Materials Advisory Services Ltd.; 1995.

[19] Overend M, Butchart C, Lambert H, Prassas M. The mechanical performance of laminated hybrid-glass units. Compos Struct 2014;110(1):163–73.

[20] Correia J, Valarinho L, Branco F. Post-cracking strength and ductility of glass–GFRP composite beams. Compos Struct 2011;93(9):2299–309.

[21] Glass in building – thermally toughened soda lime silicate safety glass (part 2). London: British Standards Institution; 2004.

[22] ASTM D3171-11. Standard test methods for constituent content of composite materials. West Conshohocken, PA: American Society for Testing and Materials; 2011.

[23] Barbero E. Introduction to composite materials design. Boca Raton, FL: CRC Press; 2011.

[24] CUR recommendation 96 – fiber reinforced plastics in civil engineering structures (draft for updating CUR 96:2003). Utrecht: CUR; 2012.

[25] Nhamoinesu S. Steel-glass composite panels. [PhD thesis]. UK: University of Cambridge; 2015.